ACS APPLIED MATERIALS & INTERFACES

Research Article

www.acsami.org

Chemically Crushed Wood Cellulose Fiber towards High-Performance Sodium-Ion Batteries

Fei Shen, Hongli Zhu, Wei Luo, Jiayu Wan, Lihui Zhou, Jiaqi Dai, Bin Zhao, Xiaogang Han, Kun Fu, and Liangbing Hu*

Department of Materials Science and Engineering, University of Maryland College Park, College Park, Maryland 20742, United States

Supporting Information

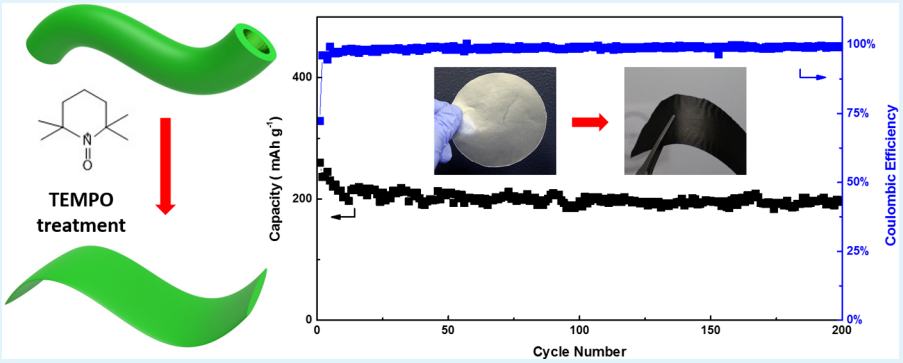

ABSTRACT: Carbon materials have attracted great interest as an anode for sodium-ion batteries (SIBs) due to their high performance and low cost. Here, we studied natural wood fiber derived hard carbon anodes for SIBs considering the abundance and low cost of wood. We discovered that a thermal carbonization of wood fiber led to a porous carbon with a high specific surface area of 586 m^2 g^{-1}, while a pretreatment with 2,2,6,6-tetramethylpiperidine-1-oxyl (TEMPO) could effectively decrease it to 126 m^2 g^{-1}. When evaluating them as anodes for SIBs, we observed that the low surface area carbon resulted in a high initial Coulombic efficiency of 72% compared to 25% of the high surface area carbon. More importantly, the low surface area carbon exhibits an excellent cycling stability that a desodiation capacity of 196 mAh g^{-1} can be delivered over 200 cycles at a current density of 100 mA g^{-1}, indicating a promising anode for low-cost SIBs.

KEYWORDS: *wood cellulose, sodium-ion batteries, carbon anode, high Coulombic efficiency, long life*

INTRODUCTION

Lithium-ion batteries (LIBs) have occupied the power source market for portable electronic devices and incoming electric vehicles (EVs) because of their high energy density and stable performance over long-term cycles.[1−3] However, the scarcity and uneven distribution of lithium resources significantly limit the further extension of LIBs. Therefore, the past few years have witnessed great growth of the research interest in alternative energy storage technologies, for example, sodium-ion batteries (SIBs).[4−6] The main advantages of SIBs are the abundance and wide availability of sodium resources, making SIBs one of the most cost-effective ways for grid-scale energy storage application.[7] In the past few years, researchers focused on developing cathodes for SIBs from the well-established LIB technology.[8−12] However, developing high-performance anodes for SIBs is still an urgent issue. The commercial anode for LIBs, graphite, has shown a very limited capacity for SIBs, owing to the large size of Na^+ ions.[13−15] As a result, many efforts are underway to find effective anodes for SIBs.

Despite various anode choices, such as alloys,[16−20] metal oxides,[21−25] and organic compounds,[26−28] carbon-based materials are still most attractive due to their high capacity, low potential, and low cost.[29−32] Among different types of carbons, hard carbon has shown promising performance in many studies after being first reported by Dahn's group.[33] However, the hard carbon anode still faces two major barriers: low initial Coulombic efficiency (CE) and poor cycling performance. To address the low initial CE, considerable efforts have been made. For example, surface modifying can increase the initial CE by reducing the contact area of carbon anode with electrolyte.[34,35] Although irreversible Na trapping in hard carbon anodes can also lead to a certain initial CE loss,[30] it is generally believed that hard carbon with a low surface area can give a high initial CE. However, controlling the cost of the carbon precursors and minimizing the surface area of hard carbon remain a significant challenge.

Cellulose is the most abundant and also renewable resource on Earth, which has attracted great interest as a carbon precursor. In this study, wood cellulose fibers derived hard carbons have been successfully developed as anodes for SIBs.

Received: August 16, 2015
Accepted: October 5, 2015
Published: October 5, 2015

DOI: 10.1021/acsami.5b07583
ACS Appl. Mater. Interfaces 2015, 7, 23291−23296

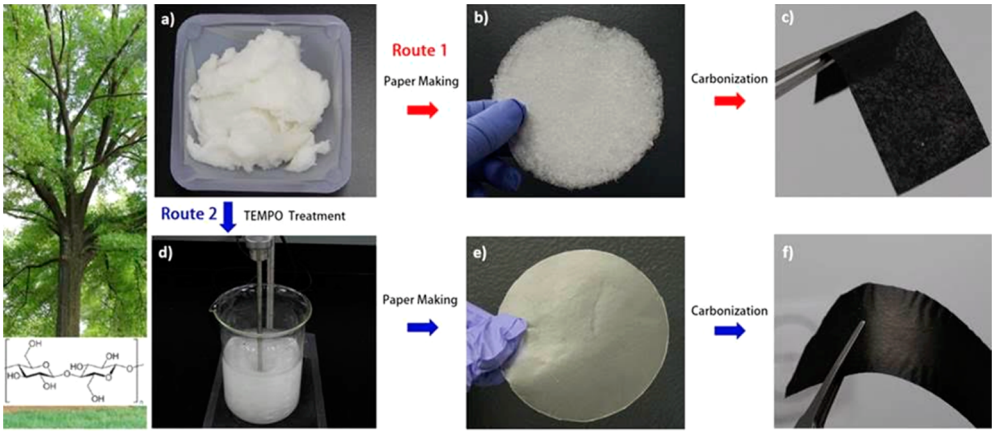

Figure 1. Steps of achieving two types of carbonized paper. In route 1, (a) natural wood fiber was directly used to make a (b) paper and (c) further carbonized to obtain pristine carbon paper. In route 2, the wood fiber was first oxidized by (d) TEMPO treatment, and then made into (e) a paper and carbonized to obtain (f) oxidized carbon paper. Route 2 leads to a much denser paper and carbonized carbon, which is more suitable for SIB anode applications.

Before the thermal carbonization of wood cellulose fiber, we conducted an oxidization using 2,2,6,6-tetramethylpiperidine-1-oxyl (TEMPO), which is a well-known technology in nanofibrillation of cellulose.[36−38] For the first time, we discovered that the surface area of the wood fiber derived hard carbon can be decreased to 126 $m^2\ g^{-1}$ by using TEMPO treatment, in sharp contrast to directly carbonized wood fiber (586 $m^2\ g^{-1}$). As expected, when evaluating as an anode for SIBs, the TEMPO-treated wood fiber derived low surface area hard carbon exhibited a much higher initial CE (72%) compared with pristine wood fiber derived porous carbon (25%). The strategy of achieving low surface area carbon with chemical treatment can be applied to many other biomass-based SIBs anodes.

EXPERIMENTAL SECTION

Preparation of Pristine Carbon Paper and Oxidized Carbon Paper. Natural wood fiber used in this work was from bleached pulp. Typically, 0.5 g Kraft bleached softwood pulp was slushed into 100 mL deionized water (DI water) and then mechanically stirred for 30 min at a speed of 1000 r min^{-1}. The pulp dispersion was then filtered by a vacuum filtration process through a 90 mm diameter 0.65 μm pore-sized membrane (Millipore) and dried at 80 °C, giving a pristine wood fiber paper. The oxidized wood fiber was obtained using a TEMPO-mediated oxidation method according to our previous paper.[38] Typically, catalytic amounts of TEMPO and NaBr were dissolved in the Kraft pulp dispersion. The oxidation of the wood fiber was triggered by adding 1 mmol NaClO under gentle agitation. During the oxidation process, the pH value was controlled at 10.0 by adding a 1.0 mol L^{-1} NaOH drop wisely. The entire reaction took about 2 h. After TEMPO treatment, the fibrils were thoroughly washed with DI water 3 times to remove the reaction agent before redispersion. Then, the obtained wood fiber dispersion was vacuum filtrated and dried at 80 °C, giving an oxidized wood fiber paper. The oxidized wood fiber paper was then transferred into a tube furnace and stabilized at 240 °C for 8 h before being further carbonized at 1000 °C under argon for 2 h. As a control, we also carbonized pristine wood fiber paper into carbon without using TEMPO treatment.

Materials Characterization. Nitrogen absorption measurements were obtained with a Micromeritics TriStar II 3020 analyzer at 77 K. Scanning electron microscopy (SEM) images were taken on a Hitachi SU-70 Schottky field emission gun scanning electron microscope, while high-resolution transmission electron microscope (HRTEM) images were taken from a JEOL 2100F field-emission TEM at 200 kV. X-ray diffraction (XRD) patterns were collected with a Bruker D8 Advance using Cu Kα radiation (λ = 1.5406 Å). Raman spectra were recorded using a Labram Aramis Raman spectrometer with a 633 nm He−Ne laser source.

Electrochemical Measurements. For electrochemical testing, 2025 coin cells were made by directly punching round discs out of carbonized papers as binder-free and additive-free working electrodes. The typical mass loading of the carbon electrode was 2.5 mg cm^{-2}. 1.0 mol L^{-1} $NaClO_4$ in (1:1 V/V) ethylene carbonate/diethyl carbonate served as the electrolyte, pure sodium metal as the counter electrode, and a 25 μm thick polypropylene membrane was used as the separator. Galvanostatic cycling was conducted with a land tester at different current densities and at room temperature.

RESULTS AND DISCUSSION

Natural wood fiber was adopted as a precursor in this study due to its abundance and low cost. As illustrated in Figure 1, route 2, wood fiber was first oxidized by TEMPO-mediated technology and fabricated to a paper according to our previous work.[38] Compared with pristine wood fiber paper (Figure 1b), oxidized wood fiber paper (Figure 1e) shows a much denser structure. Thermal carbonization was then employed to convert both the pristine wood fiber paper and oxidized wood fiber paper into carbon papers, which were referred to as pristine carbon paper (Figure 1c) and oxidized carbon paper (Figure 1f), respectively. Nitrogen adsorption−desorption measurements were then carried out to examine the porosity properties of the obtained carbon papers. The isotherms in Figure 2 reveal

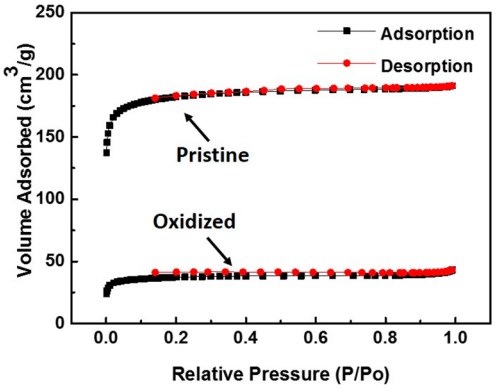

Figure 2. Nitrogen adsorption−desorption isotherms of pristine carbon paper and oxidized carbon paper.

DOI: 10.1021/acsami.5b07583
ACS Appl. Mater. Interfaces 2015, 7, 23291−23296

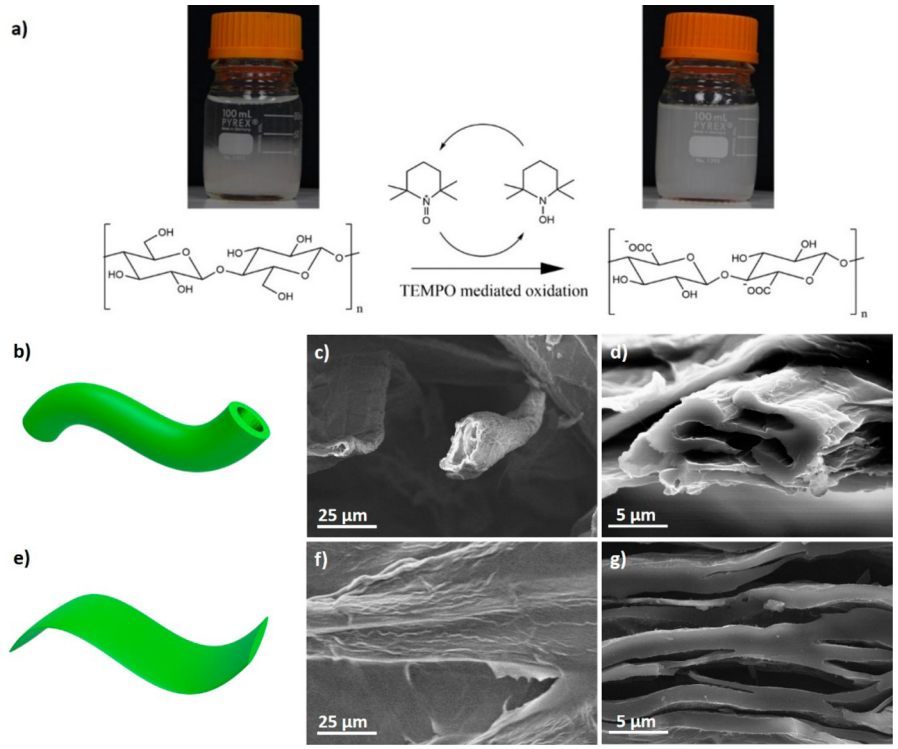

Figure 3. (a) Schematic showing TEMPO-mediated oxidation mechanism. Pristine wood fiber: (b) illustration to show hollow and hierarchical structure and (c and d) SEM images before and after carbonization, respectively. Oxidized wood fiber: (e) illustration to show ribbon-like structure and (f and g) SEM images before and after carbonization, respectively.

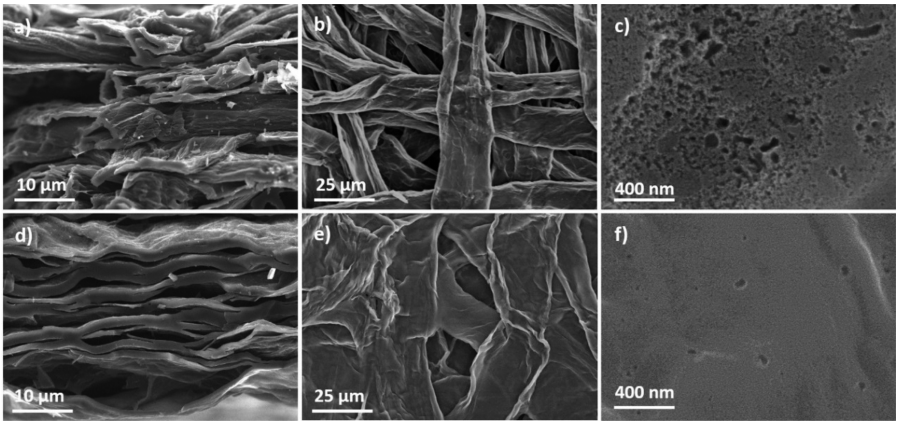

Figure 4. SEM images of (a–c) pristine carbon paper and (d–f) oxidized carbon paper.

a typical type IV behavior, and the initial steep regions indicate a certain amount of micropores existing in both carbon papers. The specific Brunauer–Emmett–Teller (BET) surface area is 586 m^2 g^{-1} for pristine carbon paper, close to those carbon materials directly derived from other biomasses.[39−41] For oxidized carbon paper, the surface area decreases sharply to 126 m^2 g^{-1}.

To investigate how the TEMPO treatment helps to minimize the surface area of carbon product, we first studied the wood fiber. Wood fiber has a unique hierarchical, hollow, and porous structure (Figure 3b). The cell walls of wood fiber are composed with bundles of cellulose microfibrils, which are constructed by 30–40 cellulose chains.[42] These mircofibrils are bonded tightly together via hydrogen bond. As demonstrated by Isogai and co-workers, TEMPO can selectively oxidize C6 hydroxyl group in the glucose unit of cellulose chain to carboxyl group (Figure 3a).[36] Thus, the TEMPO treatment loosens the hydrogen bond and induces a negative charge on the surface of microfibrils, leading to a zeta potential approximately −75 mV of the oxidized fiber.[43] Treated fiber features a ribbon-like structure (Figure 3e) due to the crush of fiber cell wall. Compared with pristine wood fiber, the TEMPO-treated wood fiber can form a more stable suspension in water due to its higher zeta potential (Figure 3a top right). SEM images were taken to give more insight into the microstructure of wood fiber before and after TEMPO oxidization. Pristine wood fiber has a large hollow chamber in the middle, and the cell wall is around a few microns, as revealed in Figure 3c. The hollow structure is not destroyed after carbonization (Figure 3d). More SEM images are given in Figure S1 to exhibit the unique hollow structure of pristine wood fiber and its resulting carbon fiber. While after TEMPO treatment, wood fibers are partially

DOI: 10.1021/acsami.5b07583
ACS Appl. Mater. Interfaces 2015, 7, 23291−23296

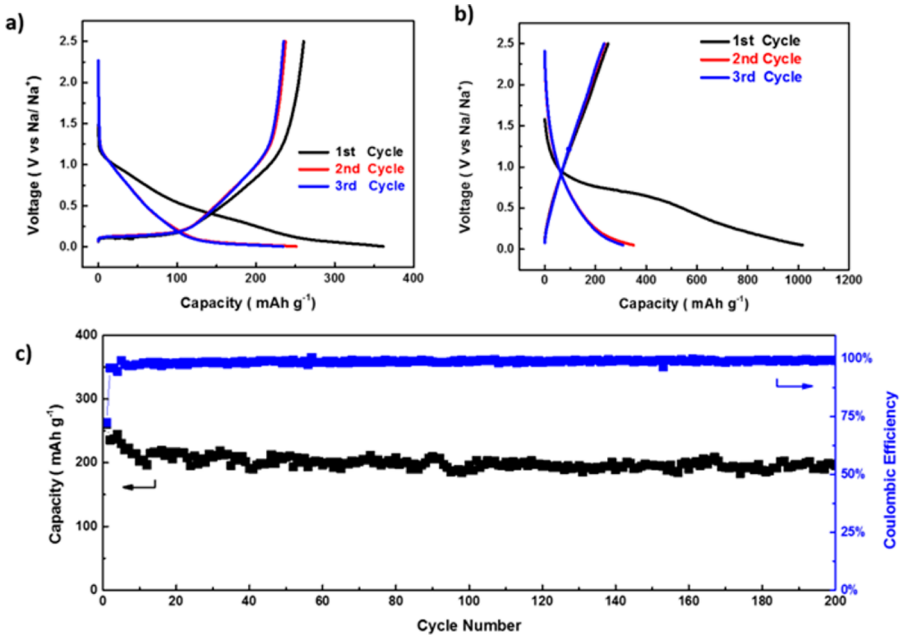

Figure 5. Potential profiles for (a) oxidized carbon paper and of (b) pristine carbon paper at 20 mA g^{-1} between the potential window of 0.01 to 2.5 V vs Na/Na^+. (c) Long-term cycling performance for oxidized carbon paper at 100 mA g^{-1}.

unzipped and form ribbon-like structure (Figure 3f). The flat nature of ribbon-like structure is well-maintained after carbonization (Figure 3g).

We further investigated the effects of different fibers on paper configuration, especially on carbonized paper. As shown in Figure S2a, numerous pristine wood fibers are randomly interwoven together and lead to a large amount of voids between these fibers. The zoomed-in image shows that these one-dimensional (1D) fibers have a typical diameter around 40 μm (Figure S2b). After TEMPO treatment, these fibers are densely packed (Figure S2c), which is sharply contrasted to the porous configuration of pristine wood fiber. The diameter of swelled fiber expands up to 100 μm (Figure S 2d). We propose that the unzipped fiber becomes ribbon-like features and is favorable to form a more compact structure. After direct carbonization, the one-dimensional (1D) hollow structure of pristine wood fiber is not destroyed in the pristine carbon paper (Figure 4, panels a and b). Many nanosized pores are generated in the pristine carbon paper (Figure 4c), which agrees well with the BET result. In oxidized carbon paper, we found ribbon-like structures which were more flat and compact than fibers in pristine carbon paper. The ribbon-like structure is initially caused by the TEMPO treatment in wood fiber and maintained after carbonization. Oxidized carbon paper also shows fewer voids between the ribbon-like features (Figure 4e). Furthermore, there are much less pores in the surface of oxidized carbon paper, suggesting a smaller surface area (Figure 4, panels e and f). More high-magnification SEM images are provided in Figure S3 to reveal that TEMPO treatment would lead a less porous surface for resulting carbon paper. In summary, pretreating wood fiber with TEMPO can partially unzip the wood fiber and create ribbon-like features. Wood fiber paper made by the ribbon-like features has a higher packing density, and a lower surface area carbon paper is further fabricated after carbonization.

To investigate the crystallinity and phase information for the products after carbonization, XRD patterns were collected. As shown in Figure S4, both pristine carbon paper and oxidized carbon paper exhibit typical amorphous carbon structure. The XRD peaks at ~23° and ~43° can readily be indexed to (002) and (101) planes, respectively. HRTEM was also carried out to analyze the crystallization behavior. Pristine carbon paper (Figure S5a) displays an amorphous structure with partially local order under 2 nm. Same disorder structure was also found in oxidized carbon paper (Figure S5b) but with more substantial short-range order.

Due to the excellent flexible nature, both carbon papers were cut into round discs and used as binder-free, self-standing electrodes with a high mass loading (2.5 mg cm^{-2}) for assembling coin cells. Galvanostatic charge/discharge cycling was first performed between the potential window from 0.01 to 2.5 V versus Na/Na^+. Figure 5a shows the charge/discharge curves of the oxidized carbon paper for the first three cycles at a current density of 20 mA g^{-1}. Oxidized carbon paper delivers sodiation and desodiation capacities of 361 and 260 mAh g^{-1} in the first cycle, giving the initial CE up to 72%, which to our knowledge is very high among other biomass-derived carbon anodes for SIBs.[32,44,45] The potential profile of oxidized carbon paper exhibits a typical hard carbon behavior.[31] According to Dahn's "house of cards" model,[33] a sloping region from 1.0 to 0.2 V is related to Na ions intercalation into graphitic nanodomains, and a flat plateau near 0.2 V is attributed to the absorption of Na ions into nanopores. Most recently, a modified mechanism is proposed for pseudographitic carbon material that the capacity above 0.2 V is due to reversible adsorption of Na ions at nanosized defects, while the capacity below 0.2 V is Na ions intercalation between graphitic planes.[46,47] In sharp contrast, pristine carbon paper exhibits a "supercapacitor-like" slope potential profile (Figure 5b), which is due to the large surface area (586 m^2 g^{-1}). Also the sodiation and desodiation capacities were 1012 mAh g^{-1} and 252 mAh g^{-1}, respectively, giving a low initial CE of 25%. Obviously, the oxidized carbon paper exhibited a much higher initial CE, which is mainly attributed to its dense structure and lower surface area induced by TEMPO treatment. Stable cycling performance is also highly pursued for practical applications.

DOI: 10.1021/acsami.5b07583
ACS Appl. Mater. Interfaces 2015, 7, 23291−23296

Here, oxidized carbon paper electrode was further performed at 100 mA g^{-1} for 200 cycles after cycling at 20 mA g^{-1} for 5 cycles (Figure 5c). The oxidized carbon paper exhibits a stable capacity around 196 mAh g^{-1} with nearly 100% CE over 200 cycles. While for pristine carbon paper, a much lower CE around 92% is performed upon cycling (Figure S6), suggesting a continuous irreversible reaction in pristine carbon paper. Both the high initial CE and stable cycling performance indicate that the oxidized carbon paper is a very promising anode for SIBs.

CONCLUSION

In summary, we successfully devised a novel strategy to decrease the surface area of wood fiber derived hard carbon by using TEMPO treatment. This treatment can effectively crush and unzip hollow wood fiber by oxidizing the hydroxyl groups and breaking the hydrogen bond. As a result, a much denser wood fiber paper was fabricated and led to a low surface area carbon paper by following carbonization. When evaluating as an anode for SIBs, the low surface area carbon exhibited a high initial Coulombic efficiency of 72%, a high capacity of 240 mAh g^{-1}, and a stable cycling performance over 200 cycles. Our methodology to reduce the surface area of carbon anode is very competitive for a practical production. To our knowledge, enzyme and some strong acids can swell and disaggregate wood, cotton and bacterial celluloses as well, thus further investigation is being undertaken in our lab. Furthermore, our work may also give some inspiration on the pretreatment of carbon precursors for other applications.

ASSOCIATED CONTENT

Supporting Information

The Supporting Information is available free of charge on the ACS Publications website at DOI: 10.1021/acsami.5b07583.

SEM images, XRD patterns. HRTEM images, and long-term cycling data for pristine carbon paper (PDF)

AUTHOR INFORMATION

Corresponding Author

*E-mail: binghu@umd.edu.

Notes

The authors declare no competing financial interest.

ACKNOWLEDGMENTS

This work was supported as part of the Nanostructures for Electrical Energy Storage (NEES), an Energy Frontier Research Center funded by the U.S. Department of Energy, Office of Science, Basic Energy Sciences under Award DESC0001160. L. Hu was also supported by Air Force of Scientific Research (AFOSR) from Department of Defense (DOD) under Young Investigator Program (FA95501310143). F. Shen was financially supported by China Scholarship Council (CSC). We would like to thank Dr. Kang Xu for help with the electrolyte.

REFERENCES

(1) Armand, M.; Tarascon, J. M. Building Better Batteries. *Nature* **2008**, *451*, 652−657.

(2) Yuan, L. X.; Wang, Z. H.; Zhang, W. X.; Hu, X. L.; Chen, J. T.; Huang, Y. H.; Goodenough, J. B. Development and Challenges of $LiFePO_4$ Cathode Material for Lithium-Ion Batteries. *Energy Environ. Sci.* **2011**, *4*, 269−284.

(3) Simon, P.; Gogotsi, Y.; Dunn, B. Where Do Batteries End and Supercapacitors Begin? *Science* **2014**, *343*, 1210−1211.

(4) Ellis, B. L.; Nazar, L. F. Sodium and Sodium-Ion Energy Storage Batteries. *Curr. Opin. Solid State Mater. Sci.* **2012**, *16*, 168−177.

(5) Slater, M. D.; Kim, D.; Lee, E.; Johnson, C. S. Sodium-Ion Batteries. *Adv. Funct. Mater.* **2013**, *23*, 947−958.

(6) Palomares, V.; Serras, P.; Villaluenga, I.; Hueso, K. B.; Carretero-Gonzalez, J.; Rojo, T. Na-Ion Batteries, Recent Advances and Present Challenges to Become Low Cost Energy Storage Systems. *Energy Environ. Sci.* **2012**, *5*, 5884−5901.

(7) Pan, H. L.; Hu, Y. S.; Chen, L. Q. Room-Temperature Stationary Sodium-Ion Batteries for Large-Scale Electric Energy Storage. *Energy Environ. Sci.* **2013**, *6*, 2338−2360.

(8) Hong, S. Y.; Kim, Y.; Park, Y.; Choi, A.; Choi, N. S.; Lee, K. T. Charge Carriers in Rechargeable Batteries: Na Ions vs. Li Ions. *Energy Environ. Sci.* **2013**, *6*, 2067−2081.

(9) Kim, D.; Kang, S. H.; Slater, M.; Rood, S.; Vaughey, J. T.; Karan, N.; Balasubramanian, M.; Johnson, C. S. Enabling Sodium Batteries Using Lithium-Substituted Sodium Layered Transition Metal Oxide Cathodes. *Adv. Energy Mater.* **2011**, *1*, 333−336.

(10) Jian, Z. L.; Han, W. Z.; Lu, X.; Yang, H. X.; Hu, Y. S.; Zhou, J.; Zhou, Z. B.; Li, J. Q.; Chen, W.; Chen, D. F.; Chen, L. Q. Superior Electrochemical Performance and Storage Mechanism of $Na_3V_2(PO_4)_3$ Cathode for Room-Temperature Sodium-Ion Batteries. *Adv. Energy Mater.* **2013**, *3*, 156−160.

(11) Yabuuchi, N.; Kajiyama, M.; Iwatate, J.; Nishikawa, H.; Hitomi, S.; Okuyama, R.; Usui, R.; Yamada, Y.; Komaba, S. P2-Type Nax$[Fe_{1/2}Mn_{1/2}]O_2$ Made from Earth-Abundant Elements for Rechargeable Na Batteries. *Nat. Mater.* **2012**, *11*, 512−517.

(12) Zhu, H. L.; Lee, K. T.; Hitz, G. T.; Han, X. G.; Li, Y. Y.; Wan, J. Y.; Lacey, S.; Cresce, A. V.; Xu, K.; Wachsman, E.; Hu, L. B. Free-Standing $Na_{2/3}Fe_{1/2}Mn_{1/2}O_2$@Graphene Film for a Sodium-Ion Battery Cathode. *ACS Appl. Mater. Interfaces* **2014**, *6*, 4242−4247.

(13) Pascal, G. E.; Fouletier, M. Electrochemical Intercalation of Sodium in Graphite. *Solid State Ionics* **1988**, *28*, 1172−1175.

(14) Wen, Y.; He, K.; Zhu, Y. J.; Han, F. D.; Xu, Y. H.; Matsuda, I.; Ishii, Y.; Cumings, J.; Wang, C. S. Expanded Graphite as Superior Anode for Sodium-Ion Batteries. *Nat. Commun.* **2014**, *5*, 4033−4042.

(15) Nobuhara, K.; Nakayama, H.; Nose, M.; Nakanishi, S.; Iba, H. First-Principles Study of Alkali Metal-Graphite Intercalation Compounds. *J. Power Sources* **2013**, *243*, 585−587.

(16) Zhu, H. L.; Jia, Z.; Chen, Y. C.; Weadock, N.; Wan, J. Y.; Vaaland, O.; Han, X. G.; Li, T.; Hu, L. B. Tin Anode for Sodium-Ion Batteries Using Natural Wood Fiber as a Mechanical Buffer and Electrolyte Reservoir. *Nano Lett.* **2013**, *13*, 3093−3100.

(17) Han, X. G.; Liu, Y.; Jia, Z.; Chen, Y. C.; Wan, J. Y.; Weadock, N.; Gaskell, K. J.; Li, T.; Hu, L. B. Atomic-Layer-Deposition Oxide Nanoglue for Sodium Ion Batteries. *Nano Lett.* **2014**, *14*, 139−147.

(18) Xu, Y.; Zhu, Y.; Liu, Y.; Wang, C. Electrochemical Performance of Porous Carbon/Tin Composite Anodes for Sodium-Ion and Lithium-Ion Batteries. *Adv. Energy Mater.* **2013**, *3*, 128−133.

(19) Qian, J.; Chen, Y.; Wu, L.; Cao, Y.; Ai, X.; Yang, H. High Capacity Na-Storage and Superior Cyclability of Nanocomposite Sb/C Anode for Na-Ion Batteries. *Chem. Commun.* **2012**, *48*, 7070−7072.

(20) Zhu, Y. J.; Han, X. G.; Xu, Y. H.; Liu, Y. H.; Zheng, S. Y.; Xu, K.; Hu, L. B.; Wang, C. S. Electrospun Sb/C Fibers for a Stable and Fast Sodium-Ion Battery Anode. *ACS Nano* **2013**, *7*, 6378−6386.

(21) Xu, Y.; Lotfabad, E. M.; Wang, H. L.; Farbod, B.; Xu, Z. W.; Kohandehghan, A.; Mitlin, D. Nanocrystalline Anatase TiO_2: A New Anode Material for Rechargeable Sodium Ion Batteries. *Chem. Commun.* **2013**, *49*, 8973−8975.

(22) Jiang, Y. Z.; Hu, M. J.; Zhang, D.; Yuan, T. Z.; Sun, W. P.; Xu, B.; Yan, M. Transition Metal Oxides for High Performance Sodium Ion Battery Anodes. *Nano Energy* **2014**, *5*, 60−66.

(23) Cao, Y.; Xiao, L.; Wang, W.; Choi, D.; Nie, Z.; Yu, J.; Saraf, L. V.; Yang, Z.; Liu, J. Reversible Sodium Ion Insertion in Single Crystalline Manganese Oxide Nanowires with Long Cycle Life. *Adv. Mater.* **2011**, *23*, 3155−3160.

(24) Jian, Z. L.; Zhao, B.; Liu, P.; Li, F. J.; Zheng, M. B.; Chen, M. W.; Shi, Y.; Zhou, H. S. Fe2O3 Nanocrystals Anchored onto Graphene

DOI: 10.1021/acsami.5b07583
ACS Appl. Mater. Interfaces 2015, 7, 23291−23296

Nanosheets as the Anode Material for Low-Cost Sodium-Ion Batteries. *Chem. Commun.* **2014**, *50*, 1215−1217.
(25) Su, D. W.; Ahn, H. J.; Wang, G. X. SnO_2@Graphene Nanocomposites as Anode Materials for Na-Ion Batteries with Superior Electrochemical Performance. *Chem. Commun.* **2013**, *49*, 3131−3133.
(26) Park, Y.; Shin, D. S.; Woo, S. H.; Choi, N. S.; Shin, K. H.; Oh, S. M.; Lee, K. T.; Hong, S. Y. Sodium Terephthalate as an Organic Anode Material for Sodium Ion Batteries. *Adv. Mater.* **2012**, *24*, 3562−3567.
(27) Deng, W. W.; Liang, X. M.; Wu, X. Y.; Qian, J. F.; Cao, Y. L.; Ai, X. P.; Feng, J. W.; Yang, H. X. A Low Cost, All-Organic Na-Ion Battery Based on Polymeric Cathode and Anode. *Sci. Rep.* **2013**, *3*, 2671.
(28) Zhu, H.; Yin, J.; Zhao, X.; Wang, C.; Yang, X. Humic Acid as Promising Organic Anodes for Lithium/Sodium Ion Batteries. *Chem. Commun.* **2015**, *51*, 14708−14711.
(29) Li, W.; Zeng, L.; Yang, Z.; Gu, L.; Wang, J.; Liu, X.; Cheng, J.; Yu, Y. Free-Standing and Binder-Free Sodium-Ion Electrodes with Ultralong Cycle Life and High Rate Performance Based on Porous Carbon Nanofibers. *Nanoscale* **2014**, *6*, 693−698.
(30) Lotfabad, E. M.; Ding, J.; Cui, K.; Kohandehghan, A.; Kalisvaart, W. P.; Hazelton, M.; Mitlin, D. High-Density Sodium and Lithium Ion Battery Anodes from Banana Peels. *ACS Nano* **2014**, *8*, 7115−7129.
(31) Luo, W.; Schardt, J.; Bommier, C.; Wang, B.; Razink, J.; Simonsen, J.; Ji, X. Carbon Nanofibers Derived from Cellulose Nanofibers as a Long-Life Anode Material for Rechargeable Sodium-Ion Batteries. *J. Mater. Chem. A* **2013**, *1*, 10662−10666.
(32) Cao, Y.; Xiao, L.; Sushko, M. L.; Wang, W.; Schwenzer, B.; Xiao, J.; Nie, Z.; Saraf, L. V.; Yang, Z.; Liu, J. Sodium Ion Insertion in Hollow Carbon Nanowires for Battery Applications. *Nano Lett.* **2012**, *12*, 3783−3787.
(33) Stevens, D. A.; Dahn, J. R. High Capacity Anode Materials for Rechargeable Sodium-Ion Batteries. *J. Electrochem. Soc.* **2000**, *147*, 1271−1273.
(34) Li, Y. M.; Xu, S. Y.; Wu, X. Y.; Yu, J. Z.; Wang, Y. S.; Hu, Y. S.; Li, H.; Chen, L. Q.; Huang, X. J. Amorphous Monodispersed Hard Carbon Micro-Spherules Derived From Biomass as a High Performance Negative Electrode Material for Sodium-Ion Batteries. *J. Mater. Chem. A* **2015**, *3*, 71−77.
(35) Luo, W.; Bommier, C.; Jian, Z.; Li, X.; Carter, R.; Vail, S.; Lu, Y.; Lee, J.-J.; Ji, X. Low-Surface-Area Hard Carbon Anode for Na-Ion Batteries via Graphene Oxide as a Dehydration Agent. *ACS Appl. Mater. Interfaces* **2015**, *7*, 2626−2631.
(36) Isogai, A.; Saito, T.; Fukuzumi, H. TEMPO-Oxidized Cellulose Nanofibers. *Nanoscale* **2011**, *3*, 71−85.
(37) Fang, Z. Q.; Zhu, H. L.; Li, Y. Y.; Liu, Z.; Dai, J. Q.; Preston, C.; Garner, S.; Cimo, P.; Chai, X. S.; Chen, G.; Hu, L. B. Light Management in Flexible Glass by Wood Cellulose Coating. *Sci. Rep.* **2014**, *4*, 5842.
(38) Fang, Z. Q.; Zhu, H. L.; Yuan, Y. B.; Ha, D.; Zhu, S. Z.; Preston, C.; Chen, Q. X.; Li, Y. Y.; Han, X. G.; Lee, S.; Chen, G.; Li, T.; Munday, J.; Huang, J. S.; Hu, L. B. Novel Nanostructured Paper with Ultrahigh Transparency and Ultrahigh Haze for Solar Cells. *Nano Lett.* **2014**, *14*, 765−773.
(39) Xie, X. F.; Goodell, B.; Zhang, D. J.; Nagle, D. C.; Qian, Y. H.; Peterson, M. L.; Jellison, J. Characterization of Carbons Derived from Cellulose and Lignin and Their Oxidative Behavior. *Bioresour. Technol.* **2009**, *100*, 1797−1802.
(40) Zhang, L. C.; Hu, Z.; Wang, L.; Teng, F.; Yu, Y.; Chen, C. H. Rice Paper-Derived 3D-Porous Carbon Films for Lithium-Ion Batteries. *Electrochim. Acta* **2013**, *89*, 310−316.
(41) Wang, S. X.; Yang, L. P.; Stubbs, L. P.; Li, X.; He, C. B. Lignin-Derived Fused Electrospun Carbon Fibrous Mats as High Performance Anode Materials for Lithium Ion Batteries. *ACS Appl. Mater. Interfaces* **2013**, *5*, 12275−12282.
(42) Kalia, S.; Dufresne, A.; Cherian, B. M.; Kaith, B. S.; Averous, L.; Njuguna, J.; Nassiopoulos, E. Cellulose-Based Bio- and Nanocomposites: A Review. *Int. J. Polym. Sci.* **2011**, *2011*, 1−35.
(43) Okita, Y.; Saito, T.; Isogai, A. Entire Surface Oxidation of Various Cellulose Microfibrils by TEMPO-Mediated Oxidation. *Biomacromolecules* **2010**, *11*, 1696−1700.
(44) Hong, K. L.; Qie, L.; Zeng, R.; Yi, Z. Q.; Zhang, W.; Wang, D.; Yin, W.; Wu, C.; Fan, Q. J.; Zhang, W. X.; Huang, Y. H. Biomass Derived Hard Carbon Used as a High Performance Anode Material for Sodium Ion Batteries. *J. Mater. Chem. A* **2014**, *2*, 12733−12738.
(45) Ding, J.; Wang, H.; Li, Z.; Kohandehghan, A.; Cui, K.; Xu, Z.; Zahiri, B.; Tan, X.; Lotfabad, E. M.; Olsen, B. C.; Mitlin, D. Carbon Nanosheet Frameworks Derived from Peat Moss as High Performance Sodium Ion Battery Anodes. *ACS Nano* **2013**, *7*, 11004−11015.
(46) Memarzadeh Lotfabad, E.; Kalisvaart, P.; Kohandehghan, A.; Karpuzov, D.; Mitlin, D. Origin of non-SEI related coulombic efficiency loss in carbons tested against Na and Li. *J. Mater. Chem. A* **2014**, *2*, 19685−19695.
(47) Ding, J.; Wang, H.; Li, Z.; Cui, K.; Karpuzov, D.; Tan, X.; Kohandehghan, A.; Mitlin, D. Peanut shell hybrid sodium ion capacitor with extreme energy-power rivals lithium ion capacitors. *Energy Environ. Sci.* **2015**, *8*, 941−955.

DOI: 10.1021/acsami.5b07583
ACS Appl. Mater. Interfaces 2015, 7, 23291−23296